AGU PUBLICATIONS

Geophysical Research Letters

RESEARCH LETTER
10.1002/2014GL062379

Key Points:
- The West Napa earthquake changed stress on Bay Area faults
- Rapid stress-based earthquake forecasts for evaluating methods
- Forecasts will be evaluated against the actual aftershock patterns

Supporting Information:
- Readme
- Table S1

Correspondence to:
T. Parsons,
tparsons@usgs.gov

Citation:
Parsons, T., M. Segou, V. Sevilgen, K. Milner, E. Field, S. Toda, and R. S. Stein (2014), Stress-based aftershock forecasts made within 24 h postmain shock: Expected north San Francisco Bay area seismicity changes after the 2014 $M = 6.0$ West Napa earthquake, *Geophys. Res. Lett.*, *41*, doi:10.1002/2014GL062379.

Received 30 OCT 2014
Accepted 3 DEC 2014
Accepted article online 5 DEC 2014

Stress-based aftershock forecasts made within 24 h postmain shock: Expected north San Francisco Bay area seismicity changes after the 2014 $M = 6.0$ West Napa earthquake

Tom Parsons[1], Margaret Segou[2], Volkan Sevilgen[3], Kevin Milner[4], Edward Field[5], Shinji Toda[6], and Ross S. Stein[1]

[1]U.S. Geological Survey, Menlo Park, California, USA, [2]Geosciences Azur, Sophia Antipolis, France, [3]Seismicity.net, San Carlos, California, USA, [4]Southern California Earthquake Center, University of Southern California, Los Angeles, California, USA, [5]U.S. Geological Survey, Golden, Colorado, USA, [6]Tohoku University, Sendai, Japan

Abstract We calculate stress changes resulting from the $M = 6.0$ West Napa earthquake on north San Francisco Bay area faults. The earthquake ruptured within a series of long faults that pose significant hazard to the Bay area, and we are thus concerned with potential increases in the probability of a large earthquake through stress transfer. We conduct this exercise as a prospective test because the skill of stress-based aftershock forecasting methodology is inconclusive. We apply three methods: (1) generalized mapping of regional Coulomb stress change, (2) stress changes resolved on Uniform California Earthquake Rupture Forecast faults, and (3) a mapped rate/state aftershock forecast. All calculations were completed within 24 h after the main shock and were made without benefit of known aftershocks, which will be used to evaluative the prospective forecast. All methods suggest that we should expect heightened seismicity on parts of the southern Rodgers Creek, northern Hayward, and Green Valley faults.

1. Introduction

On 24 August 2014, the largest earthquake since the 1989 $M = 7.0$ Loma Prieta shock struck the San Francisco Bay area, the $M = 6.0$ West Napa event. This earthquake nucleated ~11 km beneath Napa Valley on or near the West Napa fault, which is itself one a series of subparallel right-lateral strike-slip faults that comprise the San Andreas fault system. The $M = 6.0$ earthquake injured 120 people, three critically, and caused localized damage in Napa Valley. The setting of this earthquake between the Hayward-Rodgers Creek system to the west and the Concord-Green Valley faults to the east (Figures 1 and 2) raises concerns that stress imparted by the West Napa earthquake might bring sections of these faults closer to failure, potentially triggering $M > 7$ events [e.g., *Field et al.*, 2014]. We additionally want to test stress change forecasting prospectively by making calculations on the same day of the earthquake before seeing the spatial pattern of aftershocks. While there will be more refined information about the West Napa earthquake rupture available in the future, our goal is to attempt to forecast immediate seismicity effects on surrounding faults at a variety of scales. As there is uncertainty about the most effective approach in resolving calculated stress change onto fault targets, and how best to relate them to seismicity changes [e.g., *Woessner et al.*, 2011], we try three different methods. We will revisit this prospective forecast in subsequent years to evaluate its performance based on subsequent seismicity, creep, and surface strain. We have produced stress-based forecasts following the 2005 $M = 7.6$ Kashmir and 2008 $M = 7.9$ Wenchuan earthquakes [*Parsons et al.*, 2006, 2008], subsequently evaluated their performance [*Parsons et al.*, 2012], and then reevaluated after a large aftershock to the Wenchuan event occurred in 2013 [*Parsons and Segou*, 2014].

The initial submission of this publication was recorded on 3 September 2014; two of the forecasts produced here were not advised by any aftershocks, and the third used only the first 4 h to define the rupture plane. This revised publication makes use of aftershocks through 16 October 2014 to make very preliminary evaluations of the methods but not to change the forecasts.

©2014. American Geophysical Union. All Rights Reserved.

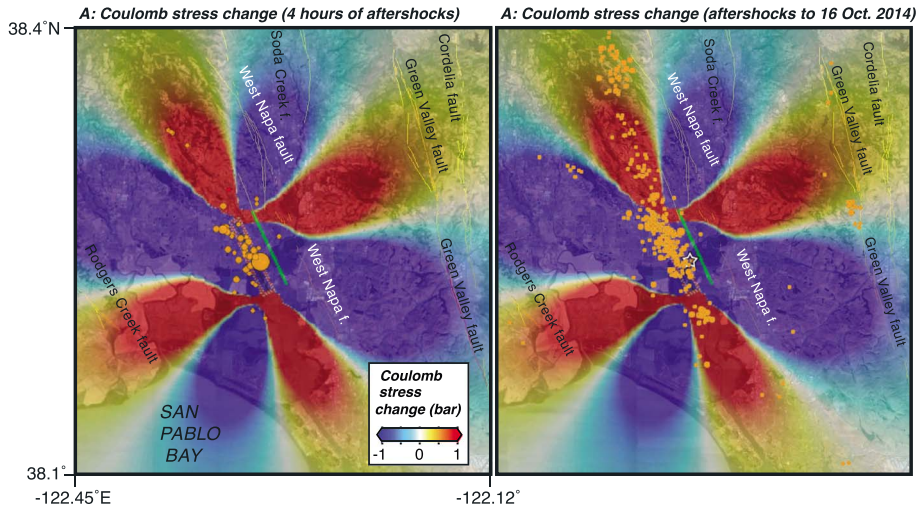

Figure 1. (a) Coulomb stress change surrounding the West Napa rupture; warm colors show calculated stress (and therefore, hazard) increase, and cool colors show decreases (stress shadows). Based on the initial seismic moment and initial 4 h of aftershocks, a 6 km × 6 km square source centered at 11 km depth with 1.3 m of slip was used to simulate the $M = 6.0$ West Napa earthquake; the surface projection of the rupture surface is shown as the dashed red rectangle; the rupture plane projects to the ground surface along the green line. The Northern California Seismic System (NCSS) centroid moment tensor (CMT) solution with 155° strike, 82° dip, and 172° rake was used for the source. For simplicity, the same geometry is assumed for all receiver faults, as they are predominantly vertical and right lateral, on which a friction coefficient of $\mu = 0.4$ was assumed at an 11 km depth. We calculate a ~0.25 bar stress increase on portions of the Green Valley and Rodgers Creek faults, and a ~0.75 bar stress decrease along most of the West Napa fault. (b) Aftershocks through 16 October 2014 are plotted.

2. Methods

Three different methods for stress-based aftershock forecasting are applied independently by different coauthors and completed within 24 h of the West Napa earthquake. All calculations are made with preliminary information about the main shock rupture, namely, the Northern California Seismic System (NCSS) centroid moment tensor (CMT) solution (http://www.ncedc.org/mt/nc72282711_MT.html), and could be readily automated for operational earthquake forecasting. The three methods evolve from (1) mapping spatial stress changes, (2) probability changes on mapped faults, and (3) an explicit, grid-based forecast seismicity rate. A stress change map by itself suggests regions where enhanced or diminished seismicity might be expected; however, many factors need to be accounted for, including magnitude of stress change, normalizing seismicity density by relative areas of stress change, and also fault source density (an area with many faults is likely to produce more earthquakes regardless of stress change). We therefore explore fault-based and grid-based methods.

2.1. Coulomb Stress Change Mapping on Generalized Fault Planes

We calculate Coulomb stress change by simulating an earthquake with a slipping dislocation in an elastic half-space [*Okada*, 1992; *Toda et al.*, 1998; *Stein*, 1999] (Figure 1). Here a 6 km by 6 km square rupture source with geometry taken from the NCSS CMT solution (155° strike, 82° dip, and 172° rake) with 1.3 m of slip centered at the hypocenter 11 km deep conserves the $M = 6.0$ West Napa earthquake moment (1.3×10^{25} dyn cm). The Coulomb criterion (ΔCFF) is defined by

$$\Delta\mathrm{CFF} \equiv |\Delta\bar{\tau}_f| + \mu'(\Delta\sigma_n - \Delta p) \tag{1}$$

where $\Delta\bar{\tau}_f$ is the change in shear stress on the receiver fault (set positive in the direction of fault slip), μ is the coefficient of friction, $\Delta\sigma_n$ is the change in normal stress acting on the target fault (set positive for unclamping), and Δp is pore pressure change. The Coulomb stress change is resolved on receiver fault planes that could have any geometry, rake, and friction. Here the receivers are assumed to have the same characteristics as the rupture source, which is consistent with the regional northwest trending strike-slip tectonics of the San Andreas fault system. The calculation in Figure 1 assumes a receiver fault friction coefficient of $\mu = 0.4$, depth of 11 km, and pore fluid effects are neglected.

©2014. American Geophysical Union. All Rights Reserved.

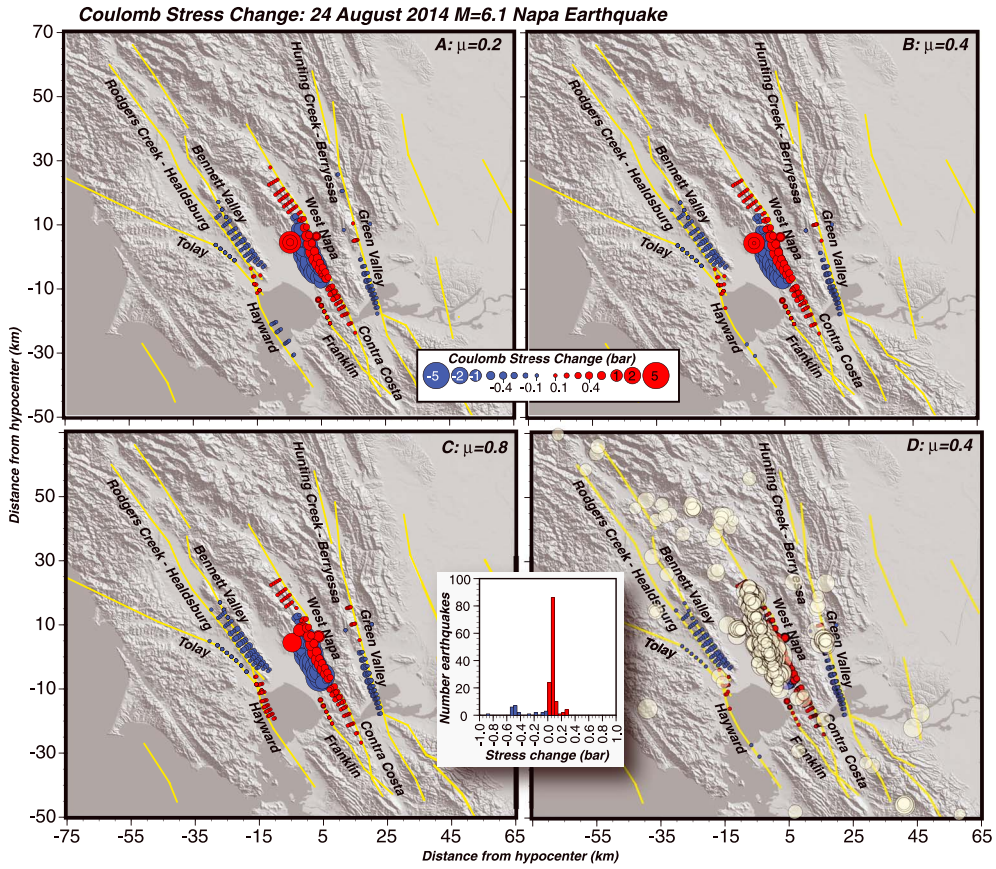

Figure 2. Coulomb stress change resolved on mapped faults defined by the Uniform California Earthquake Rupture Forecast Version 3 (UCERF3). Red dots correspond to calculated stress increases, whereas blue dots correspond to calculated decreases. Dots are located at centers of receiver fault patches (~3 km × 3 km); dipping faults are thus wider in map view. (a–c) Regardless of friction coefficient used, we find that the Hayward-Rodgers Creek fault junction, the Franklin fault, the Contra Costa shear zone, and the West Napa fault have calculated stress increases. (d) Aftershocks through 16 October 2014 are plotted, and the inset histogram shows the distribution of aftershocks associated (within ±3 km) with fault planes that have calculated stress increases or decreases.

Stress change mapping provides an estimate of the time-independent, spatial distribution of future seismicity. Therefore, the prediction is that aftershocks will preferentially occur in areas of calculated stress increase and will be less likely in calculated stress-decreased areas. This can be readily tested against the observed pattern of seismicity density at any time over the duration of aftershocks after accounting for background rates and fault distribution [e.g., *Parsons et al.*, 2012; *Parsons and Segou*, 2014].

2.2. Coulomb Stress Resolved on Mapped Fault Planes

An alternative approach to stress change calculation focuses on mapped faults. This technique is less likely to capture the complete spatial pattern of aftershocks but appears to be effective at forecasting higher magnitude earthquakes [*Parsons et al.*, 2012]. We work with faults defined by the Uniform California Earthquake Rupture Forecast Version 3 (UCERF3) [*Dawson*, 2013], which have geometries and rakes determined through a geological consensus process, and have calculated long-term $M > 5.5$–6.0 rupture rates [*Field et al.*, 2014]. Receiver faults are divided into ~3 km by ~3 km patches, and Coulomb stress is resolved on each (Figure 2). The receiver fault friction coefficient is almost impossible to know even in detailed studies, so a range is used here from $\mu = 0.2$ to $\mu = 0.8$. We use the NCSS CMT solution parameters for the main shock slip model modified slightly to match the UCERF3 geometry for the West Napa fault (155° strike, 75° dip, and 180° rake). We centered the source dislocation at the initial reported hypocenter depth of 10.7 km and scaled its dimensions using the regressions of *Wells and Coppersmith* [1994] for strike-slip rupture length (16 km), width (7.7 km), and average slip (0.15 m) at depth for a $M = 6.0$ earthquake.

©2014. American Geophysical Union. All Rights Reserved.

We assess the impact of the West Napa earthquake by calculating earthquake probability changes on major faults. A stress change can theoretically advance or delay earthquakes by time T', which can be calculated by dividing the stress change (ΔCFF) by the tectonic stressing rate ($\dot{\tau}$), as $T' = \Delta\tau/\dot{\tau}$. Time-dependent probability calculations can be adjusted by accruing probability from the last earthquake time modified by the advance or delay ($T_0 + T'$). Alternatively, the earthquake recurrence interval ξ can be adjusted by the clock change as $\xi = \xi_0 - T'$. We use the latter approach since the last earthquake time is unknown for north Bay Area faults. We use the central value of $\mu = 0.4$ for calculating ΔCFF for probability changes since it is close to the average.

To explain Omori law transient earthquake rate changes with rate/state theory, *Dieterich* [1994] derived an expression for time-dependent seismicity rate $R(t)$, after a stress perturbation as

$$R(t) = \frac{r}{\left[\exp\left(\frac{-\Delta\mathrm{CFF}}{a\sigma}\right) - 1\right]\exp\left[\frac{-t}{t_a}\right] + 1} \tag{2}$$

where r is the steady state seismicity rate, ΔCFF is the stress step, σ is the normal stress, a is a fault constitutive constant, and t_a is an observed or inferred aftershock duration. We assume t_a to be 10 years and derive the $a\sigma$ parameter from $a\sigma = t_a \cdot \dot{\tau}$ [*Dieterich*, 1994], which yields values between 0.25 and 0.5 bars based on loading rates from *Parsons* [2002] and is consistent with the 0.5 bar value of *Toda et al.* [2005].

The transient earthquake rate $R(t)$ after a stress step can be related to earthquake probability over the interval Δt as

$$P(t, \Delta t) = 1 - \exp\left[-\int_t^{t+\Delta t} R(t)\mathrm{d}t\right] = 1 - \exp(-N(t)), \tag{3}$$

[*Dieterich and Kilgore*, 1996], where $N(t)$ is the expected number of earthquakes in the interval. The transient probability change can be superimposed on recurrence interval change. Integrating for $N(t)$ yields

$$N(t) = r_p\left\{\Delta t + t_a \ln\left[\frac{1 + \left[\exp\left(\frac{-\Delta\mathrm{CFF}}{a\sigma}\right) - 1\right]\exp\left[\frac{-\Delta t}{t_a}\right]}{\exp\left(\frac{-\Delta\mathrm{CFF}}{a\sigma}\right)}\right]\right\} \tag{4}$$

where r_p is the expected rate of earthquakes associated with the permanent probability change [*Toda et al.*, 1998]. This rate can be determined by applying a stationary Poisson probability expression as

$$r_p = \left(\frac{-1}{\Delta t}\right)\ln(1 - P_c) \tag{5}$$

where P_c is a conditional probability and can be calculated using any distribution. The time-dependent Brownian Passage Time (BPT) model is used here [*Matthews et al.*, 2002], with a fixed aperiodicity of 0.5, and recurrence intervals from *Field et al.* [2014]. No dates of past large earthquakes are known for north San Francisco Bay region faults, so we use the method of *Field and Jordan* [2014] to account for unknown time of last event before an historical open interval (t_H = A.D. 1776 for the San Francisco Bay region, *Working Group on California Earthquake Probabilities* [2003]) as

$$P(\Delta t | t > t_H) = \frac{\Delta t - \int_{t_H}^{t_H+\Delta t} F(t)\mathrm{d}t}{\int_{t_H}^{\infty}[1 - F(t)]\mathrm{d}t}, \tag{6}$$

where $F(t)$ is the probability density function (BPT in this case).

We can use this expression to calculate time-dependent probability for any duration; we give values for 1 and 5 year spans on each fault subsection (length equal to half downdip width) that has a stress change magnitude $\geq$0.1 bar (Table 1). Probabilities are for events equal to or greater than the minimum magnitude for which we have rate information ($M \sim 6$). Evaluation of these calculations depends on an event of this magnitude occurring.

2.3. Coulomb and Rate/State Aftershock Forecasting

We lastly combine Coulomb stress changes and rate/state equations [*Dieterich*, 1994] to map expected seismicity rates following the stress perturbation from the West Napa event. To model the evolution of seismicity, we calculate Coulomb stress change on a 2.5 km by 2.5 km grid at target depth 10 km imparted by the West Napa earthquake for optimally oriented planes (friction varying over $\mu = 0.2$ to $\mu = 0.8$), with a regional stress field representation taken from *Hardebeck and Michael* [2004], with the maximum compressive stress set to N19°E at a differential stress magnitude of $\sigma 1 - \sigma 3 = 10$ MPa [*Toda et al.*, 2005]. We make a second

©2014. American Geophysical Union. All Rights Reserved.

Table 1. Earthquake Probability Change Values Averaged Across UCERF3 Subsections; Values Are for $M \geq M_{min}$ as Given for Each Fault[a]

			One Year Probability (%) $M \geq M_{min}$			Five Year Probability (%) $M \geq M_{min}$		
UCERF3 Fault	M_{min}	ΔCFF (bar)	BPT	Interaction	Δ	BPT	Interaction	Δ
Bennett Valley −	6.00	−0.17	0.09	0.04	−59	0.45	0.21	−55
Bennett Valley +	6.00	0.13	0.09	0.15	64	0.46	0.68	48
Contra Costa Shear Zone (Connector)	6.22	0.12	0.06	0.12	89	0.31	0.51	65
Franklin	6.25	0.21	0.06	0.15	141	0.32	0.59	89
Green Valley −	5.54	−0.26	0.36	0.17	−54	1.80	0.92	−50
Green Valley +	5.76	0.15	0.43	0.76	77	2.13	3.39	59
North Hayward −	6.04	−0.10	0.34	0.28	−18	1.68	1.43	−15
North Hayward +	6.12	0.16	0.30	0.48	62	1.48	2.17	47
Hunting Creek-Berryessa	5.86	−0.10	0.31	0.21	−33	1.56	1.12	−29
Rodgers Creek-Healdsburg −	6.18	−0.13	0.32	0.18	−44	1.59	0.97	−39
Rodgers Creek-Healdsburg +	6.17	0.13	0.30	0.50	65	1.52	2.27	49
West Napa −	6.30	−1.64	0.11	0.00	−99	0.55	0.01	−99
West Napa +	6.30	1.17	0.12	0.21	83	0.59	0.94	61

[a]Average stress change values are given for each fault; most of the faults have significant areas of positive and negative stress change (Figure 2), so the names are given with a "+" or "−" symbol, respectively. "BPT" refers to time-dependent probability using Brownian Passage Time distribution with no interactions, whereas "interaction" includes the recurrence interval change and rate/state transient effects. "Δ" is the probability change factor, calculated as $(P_{interaction} - P_{BPT})/P_{BPT}$.

calculation under an assumption that all receiver faults on the grid have properties akin to the Hayward fault (strike = N34°W, dip = 90°, and rake = 180°) (Figures 3a and 3b). We include uncertainty in receiver fault friction over a range of $\mu = 0.2$ to $\mu = 0.8$.

Under rate/state theory, a stress perturbation (ΔCFF) causes the state variable of the system γ_{n-1} before the event to evolve coseismically to a new value γ_n,

$$\gamma_n = \gamma_{n-1} \exp\left(\frac{-\Delta \mathrm{CFF}}{a\sigma}\right) \tag{7}$$

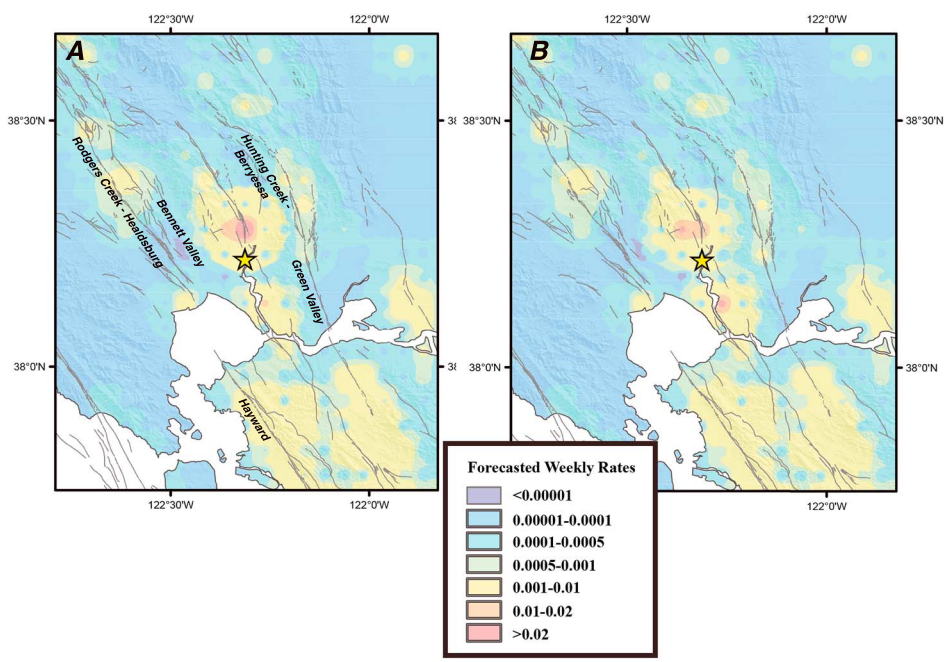

Figure 3. (a) Forecast first week of $M \geq 3.0$ seismicity rate density following the West Napa earthquake based on Coulomb stresses calculated on a grid of optimally oriented planes (friction coefficient $\mu = 0.4$) and (b) a grid of faults with Hayward fault characteristics (strike = N34°W, dip = 90°, and rake = 180°).

©2014. American Geophysical Union. All Rights Reserved.

The forecast seismicity rate R is then found from

$$R = \frac{r}{\gamma \dot{\tau}}. \tag{8}$$

This model depends on three parameters: (1) the reference seismicity rate r (background seismicity rate), which is taken from $M \geq 3.0$ rates during a 1974–2014.235 period, (2) the mean secular fault loading rate on all faults surrounding the rupture ($\dot{\tau}$ = 0.05 bar/yr) [*Parsons*, 2002], and (3) the $a\sigma$ term, taken to be 0.5 bar after *Toda et al*. [2005]. We estimate expected $M \geq 3.0$ seismicity at each node for the first week after the main shock.

3. Results

3.1. Results From Coulomb Stress Change Mapping

The mapping in Figure 1 shows broad regions of calculated stress increases and decreases that affect major fault zones north of San Francisco Bay. In particular, we calculate a ~0.25 bar stress increase on the southern Rodgers Creek fault where it enters San Pablo Bay and steps west onto the northern Hayward fault. Additionally, portions of the Green Valley fault also are calculated to have a ~0.25 bar increase; the Green Valley fault is the northern extent of the potentially linked Concord fault system that runs east of the San Francisco Bay area. We calculate a ~0.75 bar stress decrease on most of the West Napa fault.

At the time of the calculations we wrote in the initial draft of this paper: "The simplified rupture model we used for the 2014 $M = 6.0$ West Napa earthquake means that we are unlikely to capture near-source aftershock activity very accurately, and this map should instead be interpreted for expected activity on adjacent faults." This is shown by the aftershock pattern as of 16 October 2014 (Figure 1b), where many near-source aftershocks are located in the stress-reduced area around the main shock, whereas more distant events occur primarily in the stress-increased lobes.

3.2. Results From Coulomb Stress Changes Resolved on UCERF3 Faults

The spatial pattern of Coulomb stress changes resolved on individual faults in Figure 2 is comparable to the generalized mapping in Figure 1 because most of the major faults are parallel to the West Napa earthquake source. In this case we used a larger area source model with an order-of-magnitude lower average slip, meaning that we calculate stress changes over a broader spatial extent, but with lower magnitudes in most places (Figure 2). We do note some additional effects; most importantly for hazard implications, we calculate a ~0.2 bar stress increase on the northern part of the Hayward fault, and a ~0.1 bar increase on the southern Rodgers Creek fault. We find a ~0.2 bar increase on parts of the Franklin and Green Valley faults, and a ~0.1 bar increase on the Contra Costa shear zone. Strong stress increases and decreases (between 1 and 2 bar) are calculated on the West Napa fault, though uncertainty about the exact location of the main shock rupture affects near-source stress calculations. We find that if we associate aftershocks with fault surfaces (defined as being ±3 km from 3-D fault plane), then 127 aftershocks that occurred through 16 October 2014 are associated with calculated stress increases versus 24 that are associated with stress decreases (Figure 2d).

Annual and 5 year time-dependent (BPT) probability calculations are made for each fault subsection with and without stress interaction from the West Napa event. Annual probability is generally low ($<$ 1%) and not significantly different than Poisson because of the short duration, but is strongly affected (~10–50% changes) by stress changes (Table 1). Values are given for every subsection in the supporting information. We suggest that these probability values are best utilized in a relative sense because the probability of a $M \sim 6$ earthquake striking over a 1–5 year period are always low in the Bay Area; given that the Green Valley, North Hayward, and south Rodgers Creek faults would be considered the most dangerous in the aftermath of the West Napa earthquake.

3.3. Results From Coulomb/Rate-State Aftershock Forecasting

We make direct $M \geq 3.0$ aftershock forecasts based on Coulomb stress change mapping in Figure 3. The two calculations based on optimal versus regionally aligned receiver faults are similar enough to discuss concurrently. We calculate that the highest expected weekly rate (≥0.02) of $M \geq 3.0$ earthquakes will be on the Green Valley fault northeast of the rupture zone (Figure 3). We also calculate relatively lower but increased $M \geq 3.0$ rates above background (up to 0.01/week) on the Hayward, Rodgers Creek, and Bennett Valley faults.

©2014. American Geophysical Union. All Rights Reserved.

Rates calculated from stress-based methods tend to underpredict compared with observed values during the earliest phases of the aftershock period, primarily because reference background rates tend to be low, as the observation periods are not long enough to be fully representative [e.g., *Segou et al*., 2013].

We evaluate the performance of the models using log-likelihood statistics [*Schorlemmer et al*., 2007], and we find that the models underestimate the number of observed events with $\delta_1 = 3.03 \times 10^{-6}$, and $\delta_2 \cong 1$, and they are rejected within the first week. The spatial performance of the models is similar with small differences in joint log likelihood, δjLLH = 0.0038 and average LLH value of -0.32. However, a preliminary retrospective parameter optimization procedure, often used in statistical forecasting [e.g., *Werner et al*., 2011], reveals that a stressing rate for the Napa Fault of ~0.005 bar/yr leads to a successful performance evaluation. This implies that a short learning period might enable better forecast results.

4. Conclusions

We forecast future seismicity from three stress-based methods for short (1 week) to intermediate (1–5 years) using information available within the first 24 h after a main shock. The purpose is to evaluate whether rapid, physics-based methods should have any role in operational forecasts. All three methods lead to similar conclusions. Earthquake rate increases are likely on parts of the Green Valley, Franklin, Contra Costa, southern Rodgers Creek, and northern Hayward faults as a result of the 24 August 2014 $M = 6.0$ West Napa earthquake. Earthquake rate decreases are also expected on parts of the Bennett Valley, Green Valley, Hayward, and Rodgers Creek faults. Initial results suggest that stress changes are consistent with the spatial pattern of aftershocks, though a spatial rate/state forecast was rejected within the first week, and requires a learning period to adjust stressing rate parameters. We will evaluate the longer-term forecasts using observed seismicity rate changes, creep, and surface strain.

Acknowledgments
We accessed the event page for the 24 August 2014 $M = 6.0$ West Napa earthquake at http://earthquake.usgs.gov/earthquakes/eventpage/nc72282711#scientific for rapid CMT information from NCSS. We thank Editor Andrew Newman and two anonymous reviewers.

The Editor thanks John McCloskey and an anonymous reviewer for their assistance in evaluating this paper.

References

Dawson, T. E. (2013), Appendix A—Updates to the California reference fault parameter database—Uniform California Earthquake Rupture Forecast, version 3 fault models 3.1 and 3.2, *U.S. Geol. Surv. Open File Rep., 2013–1165*, 66 pp. [Available at http://pubs.usgs.gov/of/2013/1165/pdf/ofr2013-1165_appendixA.pdf.]

Dieterich, J. (1994), A constitutive law for rate of earthquake production and its application to earthquake clustering, *J. Geophys. Res.*, *99*, 2601–2618, doi:10.1029/93JB02581.

Dieterich, J. H., and B. Kilgore (1996), Implications of fault constitutive properties for earthquake prediction, *Proc. Natl. Acad. Sci. U.S.A.*, *93*, 3787–3794.

Field, E. H., and T. H. Jordan (2014), Time-dependent renewal-model probabilities when date of last earthquake is unknown, *Bull. Seismol. Soc. Am.*, in press.

Field, E. H., et al. (2014), Uniform California Earthquake Rupture Forecast, version 3 (UCERF3)—The time-independent model, *Bull. Seismol. Soc. Am.*, *104*, 1122–1180, doi:10.1785/0120130164.

Hardebeck, J. L., and A. J. Michael (2004), Stress orientations at intermediate angles to the San Andreas fault, California, *J. Geophys. Res.*, *109*, B11303, doi:10.1029/2004JB003239.

Matthews, M. V., W. L. Ellsworth, and P. A. Reasenberg (2002), A Brownian model for recurrent earthquakes, *Bull. Seismol. Soc. Am.*, *92*, 2233–2250.

Okada, Y. (1992), Internal deformation due to shear and tensile faults in a half-space, *Bull. Seismol. Soc. Am.*, *82*, 1018–1040.

Parsons, T. (2002), Post-1906 stress recovery of the San Andreas fault system from 3-D finite element analysis, *J. Geophys. Res.*, *107*(B8), 2162, doi:10.1029/2001JB001051.

Parsons, T., and M. Segou (2014), Stress, distance, magnitude, and clustering influences on the success or failure of an aftershock forecast: The 2013 $M = 6.6$ Lushan earthquake and other examples, *Seismol. Res. Lett.*, *85*, 44–51, doi:10.1785/0220130100.

Parsons, T., R. S. Yeats, Y. Yagi, and A. Hussain (2006), Static stress change from the 8 October, 2005 $M = 7.6$ Kashmir earthquake, *Geophys. Res. Lett.*, *33*, L06304, doi:10.1029/2005GL025429.

Parsons, T., C. Ji, and E. Kirby (2008), Stress changes from the 2008 Wenchuan earthquake and increased hazard in the Sichuan basin, *Nature*, *454*, 509–510, doi:10.1038/nature07177.

Parsons, T., Y. Ogata, J. Zhuang, and E. L. Geist (2012), Evaluation of static stress change forecasting with prospective and blind tests, *Geophys. J. Int.*, *188*, 1425–1440, doi:10.1111/j.1365-246X.2011.05343.x.

Schorlemmer, D., M. C. Gerstenberger, S. Wiemer, D. D. Jackson, and D. A. Rhoades (2007), Earthquake likelihood model testing, *Seismol. Res. Lett.*, *78*(1), 17–29, doi:10.1785/gssrl.78.1.17.

Segou, M., T. Parsons, and W. Ellsworth (2013), Evaluation of combined physics based and statistical forecast models, *J. Geophys. Res. Solid Earth*, *118*, 6219–6240, doi:10.1002/2013JB010313.

Stein, R. S. (1999), The role of stress transfer in earthquake occurrence, *Nature*, *402*, 605–609.

Toda, S., R. S. Stein, P. A. Reasenberg, J. H. Dieterich, and A. Yoshida (1998), Stress transferred by the 1995 $M_w = 6.9$ Kobe, Japan, shock: Effect on aftershocks and future earthquake probabilities, *J. Geophys. Res.*, *103*, 24,543–24,565, doi:10.1029/98JB00765.

Toda, S., R. S. Stein, K. Richards-Dinger, and S. Bozkurt (2005), Forecasting the evolution of seismicity in southern California: Animations built on earthquake stress transfer, *J. Geophys. Res.*, *110*, B05S16, doi:10.1029/2004JB003415.

Wells, D. L., and K. J. Coppersmith (1994), New empirical relationships among magnitude, rupture length, rupture width, rupture area, and surface displacement, *Bull. Seismol. Soc. Am.*, *84*, 974–1002.

©2014. American Geophysical Union. All Rights Reserved.

Werner, M. J., A. Helmstetter, D. D. Jackson, and Y. Y. Kagan (2011), High-resolution long-term and short-term earthquake forecasts for California, *Bull. Seismol. Soc. Am.*, *101*, 1630–1648.

Woessner, J., S. Hainzl, W. Marzocchi, M. J. Werner, A. M. Lombardi, F. Catalli, B. Enescu, M. Cocco, M. C. Gerstenberger, and S. Wiemer (2011), A retrospective comparative forecast test on the 1992 Landers sequence, *J. Geophys. Res.*, *116*, B05305, doi:10.1029/2010JB007846.

Working Group on California Earthquake Probabilities (2003), Earthquake probabilities in the San Francisco Bay region: 2002–2031, *U.S. Geol. Surv. Open File Rep.*, *03-214*, 235 pp.

©2014. American Geophysical Union. All Rights Reserved.